Functional Electro-materials Based on Ferricyanide Redox-active Ionic Liquids

Functional Electro-materials Based on Ferricyanide Redox-active Ionic Liquids

Andrew P. Doherty[a,*], Louise Graham [a,], Klaudia Wagner[b], David L. Officer[b], Jun Chen[b] and Gordon G. Wallace[b]

[a, *] School of Chemistry and Chemical Engineering, The Queens's University of Belfast, Belfast, Northern Ireland, BT9 5AG, United Kingdom.
e-mail a.p.doherty@qub.ac.uk, telephone + 44 (0)2890974481, fax + 44 (0)28906524

[b] Intelligent Polymer Research Unit, Australian Research Council Centre of Excellence for Electromaterials Science, University of Wollongong, Wollongong, NSW, Australia

Abstract

The unique physical and chemical properties of conventional room temperature ionic liquids (RTILs) render them highly deployable materials in electrochemical devices performing functions such as solvent-free electrolytes in capacitors, batteries and sensors. However, these non-faradaic applications can be complimented by incorporating faradaic redox functionality into the ionic liquid structure which facilitates access to a large array of new electrochemical applications such as dye sensitised solar cells, redox batteries, hydrid capacitors and selective amperometric sensor applications which are all reliant on heterogeneous or homogenous electron-transfer processes. This paper presents and discuses some examples of redox active ionic liquids base on the ferri-/ferro- functionality. These functional electro-materials which are already known [Ref. 18] exhibit simple reversible one-electron electrochemistry at very negative potentials (by at least -1 V relative to aqueous systems) in anhydrous media. Glass transition temperatures lower than -50 ^{o}C were also observed along with an overall thermal stability up to at least 400 ^{o}C under dry N_2 atmosphere conditions. Opportunities and challenges for these types of electro-materials are discussed.

Key words: electro-materials; task specific ionic liquids; redox active; applications; electrochemical devices

1. Introduction

The acetate ([OAc]) and tetrafluroborate ([BF_4]) salts depicted in Figure 1 are examples of the first reported air and moisture stable RTILs [1].

FIGURE 1 HERE

The introduction of these materials represented a technical step-change from the earlier unstable chloroaluminate-quaternary ammonium based molten salts [2, 3] and thus opened up a vast array of chemical and electrochemical possibilities which have been exploited ever since [4-6]. The key physical or physiochemical properties of RTILs which make them attractive for electrochemical applications include:

i) high charge carrier density (>> 1 mol L^{-1}),

ii) inherent ionic conductivity (typically mS cm^{-1} range),

iii) chemically inertness / extreme redox robustness,

iv) non-volatile / non-flammable,

v) thermal stability,

vi) liquid state at low temperatures.

The early work on RTILs concentrated on their use as “green” reaction media [4, 6] but it soon became clear that RTILs could perform useful functions (or “tasks”) such as directing the course of chemical reactions [7]. So, in addition to the favourable properties outlined above, the idea of deliberately incorporating chemical functionality into the RTIL structure to create task-specific ionic liquids (TSILs) emerged [8, 9] which has contributed greatly to the development of unique applications beyond the simple electrolytes or solvents paradigms.

It is worth noting that prior to Davis’ 2004 paper detailing Hg^{2+} sequestering TSILs, [8], examples of RTILs with built-in electro-active functionality were already known. For example, Murray et al. incorporated both quinone [10] and metal complexes [11]

into “molten salt” structures while viologen IL materials were reported in 2003 [12]. Contemporaneous to Davis [8], works by Shreeve et al. [13] and Park et al. [14] involving the incorporating of ferrocene (Fc) moieties (as functionalised cations) and I^- (as anions), respectively, were reported. Subsequently, Wu et al. [15] reported the incorporation of the redox catalyst TEMPO *(2,2,6,6*-tetramethylpiperidine-1-oxyl*)* into imidazole-based salts which, although solid in their native form at RT, were soluble in conventional ILs. More recently, Strehmel et al. [16] reported another TEMPO-based RTIL which acted as a radical probe in ILs.

It is logical that these early examples emerged from classical molecular electrochemistry and that they point in the direction of important technical applications such as enzyme redox catalysis (Fc/Fc^+), dye sensitised solar cells (I^-/I_3^-) (DSSCs), hydrogen peroxide generation / O_2 sensing (quinone/hydroquinone) and alcohol oxidations (TEMPO/nitrosonium). Presenting these, and other well-known electrochemistries, in appropriate TSIL form may lead to new or improved electrochemical technologies.

A physical feature of RTILs is their relatively large viscosities (η, g cm^{-1} s^{-1}) compared to molecular solvents. Viscosities typically range from ca. 20 cP to 1000s of cP with the common imidazolium and pyrrolidinium ILs (depending on the anion) exhibit values in the moderate 20 – 600 cP range. Deleterious effects of high viscosity include slow diffusional mass transfer rates as expressed through the Stokes-Einstein relation, and low ionic conductivities. For the latter, Gratzel et al. [17] have shown that ion conductivity (S cm^{-1}) of RTILs is an inverse function of the liquids’ bulk and micro-viscosities. Since all electrochemical devices rely on mass transport in one way or another minimising viscosity is critical.

Since viscosity is intrinsically dependent on the complexity (size, structure and structural symmetry etc.) of the cation, and the nature of the anion (e.g. H-bonding ability), the design of new functional TSILs requires appropriate careful consideration. From an intuitive empirical perspective low viscosity is achieved with small non-coordinating anions paired with larger, but not too large, structurally asymmetric cations where charge delocalisation is extensive for both ions. Even for simple RTILs, they only exist as useful liquids over a fairly narrow range of structures [19]. Obviously, adding functionality to RTILs inevitably increases mass, and frequently increases structural symmetry and inter-molecular attractive forces, all of which favour solidification; these restrictions impose severe challenges to the molecular design of TSILs.

In addition to minimising viscosity the following functional requirements must also be met for redox-active ionic liquids:

- bear a permanent charge i.e. be a RTIL irrespective of the redox state of the electro-active functionality,
- exhibit reversible electrochemistry with an E^o appropriate for the task,
- be otherwise inert,
- be either hydrophobic or hydrophilic as the application requires.

Although there are many well-known redox chemistries to choose from the syntheses, characterisation and electrochemistry of ferricyanide ($[Fe(CN)_6]^{3-}$) and ferrocyanide ($[Fe(CN)_6]^{4-}$) ILs (Figure 2) will be presented here, which follows on from earlier work [18]. Although ostensibly a simple one-electron redox couple it exhibits strong dependence on solvation and H-bonding therefore it may act as a marker for the physiochemical conditions in RTIL environments as well as being of practical importance in real electrochemical devices and processes.

FIGURE 2 HERE

2. Experimental

2.1 Synthesis of trihexyl(tetradecyl)phosphonium bis(trifluoromethanesulfonyl)imide, $[P_{14,\ 6,6,6}][NTf_2]$ ionic liquid.

In a 500 cm^3 round bottomed flask 69.04 g (0.132 mol) of trihexyl(tetradecyl)phosphonium chloride ($[P_{14,,6,6,6}][Cl]$), Cytec, USA) and 38.04 g (0.132 mol) of lithium bis(trifluoromethanesulfonyl)imide (3M) were mixed along with 170 cm^3 dichloromethane (DCM) and left to stir over night at room temperature. The LiCl precipitate was then removed by filtration (No. 4 sintered glass filter) and the resultant filtrated was washed x 6 with deionised water (DI, 18 $m\Omega\ cm^{-1}$). The DCM / $[P_{14,\ 6,6,6}][NTf_2]$ solution was then dried with anhydrous $MgSO_4$ and filtered. Finally, the DCM was removed by evaporation to produce the colourless and highly hydrophobic $[P_{14,6,6,6}][NTf_2]$ ionic liquid.

2.2 Synthesis of trihexyl(tetradecyl)phosphonium ferricyanide, $[P_{14,6,6,6}]_3[Fe(CN)_6]^{3-}$ and trihexyl(tetradecyl)phosphonium ferrocyanide, $[P_{14,6,6,6}]_4[Fe(CN)_6]^{4-}$

For $[P_{14,6,6,6}]_3[Fe(CN)_6]^{3-}$ equal volumetric quantities (10 cm^3) of acetonitrile (ACN , Sigma-Aldrich) and DI water were mixed together thoroughly (resultant volume of 17.8 cm^3) and allowed to equilibrate to room temperature after which 11.0 g (0.021 mol) of $[P_{14,,6,6,6}][Cl]$ were added with continued stirring to form a single isotropic phase. Next, 2.32 g (0.007 mol) of $K_3[Fe(CN)_6]$ (Sigma-Aldrich) were added to the $ACN/H_2O/[P_{14,6,6,6}][Cl]$ mixture whereupon an immediate ion metathesis occurred (Equation 1) as evident by a spontaneous “salting-out” driven phase separation

process that occurred forming an ACN / $[P_{14,6,6,6}]_3[Fe(CN)_6]^{3-}$ upper organic phase and an aqueous KCl (dissolved) bottom phase.

$$K_3[Fe(CN)_6] + 3\,[P_{14,6,6,6}][Cl] \longrightarrow [P_{14,6,6,6}]_3[Fe(CN)_6] + 3\,KCl\,(aq) \quad (1)$$

The organic layer was recovered using a separating funnel and the ACN removed by evaporation to produce the highly hydrophobic $[P_{14,6,6,6}]_3[Fe(CN)_6]^{3-}$ ionic liquid which was subsequently washed x 6 with DI water. Various ACN:H_2O ratios were investigated as were the effects of replacing ACN with acetone and dimethyl formamide (DMF), neither of which are reported here except for the viscosities reported in Figure 3.

For the $[P_{14,6,6,6}]_4[Fe(CN)_6]^{4-}$ synthesis, a slightly different procedure was adopted due to the limited solubility of $K_4[Fe(CN)_6].3H_2O$ in a 50:50 ACN/H_20 mixture. 2.97 g (0.0070 mol) of $K_4[Fe(CN)_6].3H_2O$ was dissolved in 10 cm^3 of DI water. 14.62 g (0.028 mol) of $[P_{14,6,6,6}][Cl]$ was dissolved in ACN. The aqueous solution was then slowly added to the ACN solution with stirring whereupon the ion metathesis reaction shown in Equation 2 occurred resulting in a spontaneous bi-phasic separation.

$$K_4[Fe(CN)_6].3H_2O + 4[P_{14,6,6,6}][Cl] \rightarrow [P_{14,6,6,6}]_4[Fe(CN)_6].3H_2O + xKCl\,(aq) + yKCl(s) \quad (2)$$

where x + y = 4.

The upper organic phase contained ACN / $[P_{14,6,6,6}]_4[Fe(CN)_6]^{4-}$ while the bottom aqueous phase was a saturated KCl solution in contact with copious quantities of KCl precipitate. The ACN layer was recovered using a separating funnel after which ACN was removed by evaporation to produce the highly hydrophobic $[P_{14,6,6,6}]_4[Fe(CN)_6]^{4-}$

ionic liquid which was subsequently washed x 6 with DI water and dried with anhydrous $MgSO_4$.

2.3 Differential Scanning Calorimetry (DSC) and Thermo-gravimetric analysis (TGA)

DSC analysis was performed using a Perkin Elmer Diamond™ DSC instrument over the temperature range -100 ^oC to 50 ^oC at temperature ramp rate of 100 ^oC / min. TGA analysis was carried out using a Mettler Toledo TGA/DSC1 Star^e instrument. The sample was heated from room temperature to 800 ^oC at 10 ^oC / min. For both techniques, the samples were held under N_2 atmosphere during measurement.

2.4 Rheological Analysis

The viscosity of $[P_{14,6,6,6}]_4[Fe(CN)_6]^{4-}$ has been reported to be 5790 cP at 20 ^oC [18]. Viscosity measurements on $[P_{14,6,6,6}]_3[Fe(CN)_6]^{3-}$ were made using a Brookfield DV-I digital viscometer fitted with a CP-52 spindle/cup that was attached to a recirculating water bath (Grant Instruments Ltd) to provide temperature control. The $[P_{14,6,6,6}]_3[Fe(CN)_6]^{3-}$ sample was further dried on a Schlenk line under high vacuum at 90 ^oC for 16 hrs prior to measurement which were carried out over the temperature range 25 $\pm$ 0.1 ^oC to 80 $\pm$ 0.1 ^oC at 5 ^oC increments. Care was taken to ensure the sample had reached equilibrium temperature before a reading was taken (*ca.* 20 mins). It was observed that the viscosity was independent of spindle rotation speed therefor readings at several different speeds at each temperature were taken and an average obtained.

2.1 Electrochemical Measurements.

All electrochemical measurements were performed using a Digi Ivy 2100 mini-potentiostat in the 3-electrode configuration. The working electrode was a 3 mm diameter glassy carbon disk (from Bioanalytical Systems (BAS)) which was polished with 0.05 μm γ-alumina as an aqueous slurry prior to use. The counter electrode was Pt wire (Goodfellow) sealed in glass. A Pt wire also acted as a quasi-reference reference electrode with added ferrocene acting as an internal potential reference. Details of electrolyte composition are given in the text and/or Figure legends as appropriate. Electrochemical characterisation was carried out on $[P_{14,6,6,6}]_3[Fe(CN)_6]^{3-}$ and $[P_{14,\ 6,6,6}]_4[Fe(CN)_6]^{4-}$ in both acetonitrile solvent (with 0.1 mol L^{-1} tetrabutyl ammonium tetrafluoroborate (TBATFB) electrolyte) and in $[P_{14,\ 6,6,6}][NTf_2]$ ionic liquid at room temperature (ca. 20 ^oC.) All solutions were sparged with dry N_2 for at least 20 minutes prior to measurement and kept under a constant N_2 blanket during measurement.

For electrochemical measurements under aqueous condition the surfactant cetyltrimethylammonium bromide (CTAB) was used to solubilise the $Fe(CN)_6]^{3-/4-}$ ILs in an aqueous electrolyte solution that was composed of 0.1 M KCl, 5.0 % (w/v) CTAB and 0.1 mol L^{-1} phosphate buffer at pH 7.4. In order to solubilise the $[P_{6,6,6,14}]_3[Fe(CN)_6]^{3-}$, and $[P_{6,6,6,14}]_4[Fe(CN)_6]^{4-}$, i.e. to form clear isotropic solutions, it was necessary to sonicated the mixtures for up to 30 minutes.

Due to uncompensated solution resistance, and the possibility of sluggish heterogeneous electron transfer kinetics, diffusion coefficients obtained from cyclic voltammetric data should be considered as indicative only.

3. Results and discussion

3.1 Viscosity measurements

Because dynamic events in liquids phases are frequently controlled by the rate of viscous flow processes the rheological properties of liquids materials is of the utmost importance – this is of particular consideration in electrochemical devices where ionic mobility, solvent reorganisation, and diffusional fluxes control the performance of the devices. The viscous behaviour of RTILs has been the subject of intense interest and scrutiny over many years [19, 20]. Seddon et al. [19] have shown that the presence of small quantities of imputes can have a dramatic effect on viscosity. Gratzel et al. [17] established the relationship between ionic conductivities and viscosities in RTILs, while Paduszyński and Domańska [20] reported the use of group contribution models for predicting RTIL viscosity. Given the large molecular mass and structural symmetry of the ferri- and ferro-cyanide ILs studied here, highly viscous behaviour is expected and, indeed, is found.

As mentioned earlier, the viscosity of $[P_{14,6,6,6}]_4[Fe(CN)_6]^{4-}$ has already been reported as 5790 cP at 20 ^oC [18]; we therefore restrict our discussion here to the viscous behaviour of $[P_{14,6,6,6}]_3[Fe(CN)_6]^{3-}$. Figure 3 shows Arrhenius plots for the viscosity of this IL prepared by four different methods, the line is for eye guidance only and is not a product of linear regression.

Figure 3 here

It is immediately evident from the data that the ILs' viscosities decrease with increasing temperature as expected, spanning values from a low 193 cP to a high of 6298 cP over the temperature range 80 ^oC to 25 ^oC. (By comparison, the starting material $[P_{14,6,6,6}][Cl]$ exhibits a viscosity of 1824 cP at 25 ^oC [21].) The change in viscosity corresponds to a physical change from being honey-like in character at room

temperature to being light oil-like at elevated temperatures. It is also evident that the ferricyanide IL's viscosity is effectively independent of the preparation method over the entire temperature range studied which is a strong indication that the materials are either relatively pure, or, at worse, have very similar impurity profiles. A closer inspection of the data also demonstrates that they exhibit slight positive curvatures suggesting that the classical hydrodynamic Arrhenius theory does not apply which is a common observation for ionic liquids and other glass forming liquids [20]. In such cases, the temperature-viscosity relationship is likely to adhere to an alternative free volume model, typically the Vogel-Tamman-Fulcher expression is assume to be appropriate [20] (VTF, Equation 3).

$$\ln \eta = A + \frac{B}{T - T_o} \qquad (3)$$

The VTF theory is based on the concept of temperature-dependent free volume, where A and B are constants and T_0 is the temperature at structural arrest which is generally considered to correspond to the glassification temperature of the liquid [22 – 24].

3.2 Thermal analysis

A review of the literature indicates that the glass transition temperature (T_g) for $[P_{14,6,6,6}][Cl]$ is -56 ^oC whilst a value of -70 ^oC has been reported for $[P_{14,6,6,6}]_4[Fe(CN)_6]^{4-}$ [18]. Table 1 shows the results of the DSC determinations of T_g for each of the four ferricyanide IL samples reported here, and for a ferrocyanide sample (synthesis by the 1 + 1 ACN + H_2O method). The values for ferricyanide are quite consistent between synthetic procedures (-54 to -51 ^oC) again indicating the samples'

purity (or similar impurity profiles). It is interesting to note that the T_g observed here for $[P_{14,\ 6,6,6}]_4[Fe(CN)_6]^{4-}$ is 14 ^oC higher than that previously reported [18] and is very similar to the ferricyanide values and to the simple chloride salt.

Table 1 here

3.3 Electrochemistry of $[P_{14,6,6,6}]_3[Fe(CN)_6]^{3-}$ and $[P_{14,6,6,6}]_4[Fe(CN)_6]^{4-}$ in molecular solvent and in ionic liquid $[P_{14,6,6,6}][NTf_2]$

$Fe(CN)_6]^{3-/4-}$ is one of the most studies redox couples and it is well know that under appropriate conditions the one-electron transfer is electrochemically reversible with formal potentials ($E^o \approx E_{1/2}$) that depend on the composition of the supporting electrolyte. For example, at neutral pH, E^o = 0.361 V vs. SHE (Standard Hydrogen Electrode) while in 0.1 mol L^{-1} HCl E^o = 0.56 V vs. SHE. It is therefore expected that the nature of the supporting electrolyte will strongly influence the electrochemical behaviour of the electroactive ionic liquids reported here.

Figure 4 shows a cyclic voltammogram for $[P_{14,6,6,6}]_3[Fe(CN)_6]^{3-}$ in ACN/ TBATFB electrolyte solution along with the potential reference compound ferrocene (Fc). It is known that the formal potential for Fc/Fc^+ is 0.64 V vs. SHE and is effectively independent of the supporting medium.

Figure 4 here

In this system, the reversible Fc/Fc^+ redox $E_{1/2}$ occurs at ca. 0.180 V vs. Pt, consistent with what is expected for the Fc/Fc^+ couple. The other redox process, although unusually distorted, with $E_{1/2}$ of ca. -1.15 V vs. Pt, can be assigned to the $Fe(CN)_6]^{3-/4-}$ redox couple. It is immediately evident that under these conditions the redox potential

for this couple has shifted to extremely negative potentials, relative to known aqueous systems. This can be seen in more detail in Figure 5 which shows cyclic voltammograms as a function of potential sweep rate (ν). These voltammograms also clearly indicate that the peak-to-peak separation increases with increasing potential sweep rate, from 90 mV to 140 mV, upon going from 5 mV/s to 200 mV/s.

Figure 5 here

Although this behaviour might be attributed to slow heterogeneous electron transfer kinetics, it is most likely due to uncompensated solution resistance (iR) within the cell since the potentiostat does not have an IR correction facility. Also evident in the voltammograms are the anodic-to-catholic peak-current ratios (I_{pa}/I_{pc}) at each potential sweep-rate that are a consistent 1.0, which, unambiguously, indicates electrochemical reversibility of $[P_{14,6,6,6}]_3[Fe(CN)_6]^3$ and very similar diffusion coefficients for both the oxidised and deuced forms. Not unexpectedly, identical electrochemical behaviour was observed for the $[P_{14,6,6,6}]_4[Fe(CN)_6]^4$ material in ACN/TBATFB electrolyte solution which can be seen in Figure 6 where the slight shift in $E_{1/2}$ is probably due to variability of the Pt quasi-reference electrode.

Figure 6 here

For both systems in ACN electrolyte, peak currents are seen to increase linearly with increasing $\nu^{1/2}$, behaviour in keeping with diffusion-controlled electrochemistry as expected. Figure 7 shows linear Randles-Sevcik plots of I_{pa} and I_{pc} vs. $\nu^{1/2}$, the slopes of which provide the mass transfer diffusion coefficients, D, for both redox forms according to the Randles-Sevcik equation (at 298 K), Equation 4.

$$I_p = 2.69x10^5\ n^{3/2}\ A\ D^{1/2}\ C\ \nu^{1/2} \quad (4)$$

where C is the concentration of the electroactive spaces and n is the number of electrons involved in the redox process. A D-value of 4.0 x 10^{-6} cm^2 s^{-1} was obtained for the ferricyanide form which is consistent with the molecular solvent's low viscosity. In addition, the near equivalence of the slopes for I_{pa} and I_{pc} suggest near equivalent mass transport rates for both redox forms.

Figure 7 here

The electrochemistry of $[P_{14,6,6,6}]_3[Fe(CN)_6]^{3-}$ and $[P_{14,6,6,6}]_4[Fe(CN)_6]^{4-}$ in $[P_{14,6,6,6}][NTf_2]$ ionic liquid is presented in Figures 8 and 9 where identical thermodynamic ($E_{1/2}$) behaviour between both samples, and between both "solvent" systems, is immediately evident. This equivalence indicates that the nature of "solvation" of the $Fe(CN)_6]^{3-/4}$ species is similar under these highly-different conditions. In addition, the equivalence of anodic and cathodic peak currents (i.e. I_{pa}/I_{pc} 1.0) is indicative of electrochemical reversibility and near equivalence of the diffusion coefficients of the respective redox couples.

Figures 8 & 9

There are, however, two significant dissimilarities with the behaviour observed in molecular solvent. Firstly, as expected, the peak-current magnitudes are at least an order of magnitude lower in the IL due to the viscosity effect. This effect can be seen

in the Randles-Sevcik plots for both materials that are shown in Figures 10 and 11 from which the corresponding D-values can be obtained. For $[P_{14,6,6,6}]_3[Fe(CN)_6]^{3-}$ a value for D of 1.0 x 10^{-8} cm^2 s^{-1} was obtained whereas for a slightly larger value of 2.0 x 10^{-8} cm^2 s^{-1} was obtained for $[P_{14,6,6,6}]_4[Fe(CN)_6]^{4-}$. Secondly, the peak-to-peak separations (ΔE_p, 150 mV to 460 mV upon going from 5 to 200 mV/s) are much larger in the ILs. In the absence of IR correction facility, the larger ΔE_p can, for the most part at least, be attributed to uncompensated solution resistant although the deleterious effect of high viscosity on electron transfer dynamics cannot be totally discounted [25].

Figures 10 & 11 here

In order to understands physiochemical origin of the very negative redox potential for the $[P_{14,6,6,6}]_{3/4}[Fe(CN)_6]^{3-/4}$ species work by Gutmann et al. [26-28] and Pletcher et al. [29] are highly informative. These workers studied the electrochemistry of $Fe(CN)_6]^{3-/4}$ in aprotic organic solvent and found the formal potentials to be *ca.* 1.0 - 1.3 V more negative in the aprotic solvents compared to aqueous values. The Authors speculated that the difference arose from a strong stabilisation of the Fe^{2+} complex by water due to the donor properties of the nitrogen in $[Fe(CN)_6]^{4-}$ being much stronger than in $[Fe(CN)_6]^{3-}$ as the Fe^{2+} is a weaker electron acceptor and also a much stronger π-electron donor. Pletcher et al. [29] further considered the following redox reaction involving a hydration / dehydration step (Equation 5)

$$Fe(CN)_6(H_2O)_p^{3-} + (q - p)\ H_2O + e^- \rightleftharpoons Fe(CN)_6(H_2O)_q^{4-} \qquad (5)$$

where q > p. If diffusion and activity coefficients are ignored, the linear behaviour can be accounted for using Nernst-like free energy function (Equation 6);

$$\Delta E^o = (E^o)_{solvent+water} - (E^o)_{solvent} = RT/F\{\log(K_{II}/K_{III}) + (q-p)\log[H_2O]\} \quad (6)$$

where K_{II} and K_{III} are the overall stability constants for the formation of the ferrocyanide/water and ferricyanide/water complexes, respectively.

In order to examine the effect of H_2O on the electrochemistry of hydrophobic $[P_{14,6,6,6}]_{3/4}[Fe(CN)_6]^{3-/4}$ ILs, aqueous solutions were prepared using the CTAB surfactant in KCl/PBS buffer. A cyclic voltammogram of $[P_{14,6,6,6}]_4[Fe(CN)_6]^{4-}$ in this medium is shown in Figure 12 where classical 1-electron reversible electrochemistry centred at ca. -0.125 V s. Pt is evident which is at least 1 V more positive than in either the ACN or the IL environments which is entirely consistent with Pletcher et al.'s [29] observations.

Figure 12 here

3.4 Stability of $[P_{14,6,6,6}]_3[Fe(CN)_6]^{3-}$ and $[P_{14,6,6,6}]_4[Fe(CN)_6]^{4-}$

It is well known that ferricyanides are prone to the adventitious formation of Prussian blue (PB, ferric hexacyanoferrate, $Fe^{III}_4[Fe^{II}(CN)_6]_3$) which, in the appropriate context, is useful; for example, as a surface-immobilised redox catalyst for H_2O_2 reduction in oxidase based biosensors such as the Glucomen Day glucose biosensor [30]). The material synthesised here are not immune to PB formation and its deposition on surfaces, although not investigated here, an ionic liquid form of PB may have useful electrochemical properties and is currently the subject of further investigation.

TGA was used to investigate the thermal stability of the $Fe(CN)_6]^{3-/4-}$ ionic liquids (and $[P_{6,6,6,14}][Cl]$ for comparative purposes) up to 800 ^oC. A number of samples exhibited weight loss at temperatures below 75 ^oC which is likely to be the loss of residual solvent or low molecular weight neutral contaminants. Overall, both $Fe(CN)_6]^{3-/4-}$ liquids exhibited excellent thermal stabilities with the materials remaining stable up to at least 400 ^oC. Onset decomposition temperatures, T_{onset}, defined as the temperature at which decomposition begins to occur, are shown in Table 1. It is clear that the phosphonium cation of $[P_{14,6,6,6}][Cl]$ decomposes at 425 ^oC which compares favourably with the T_{onset} for the two $Fe(CN)_6]^{3-/4-}$ ionic liquids samples, i.e. 413 ^oC and 431 ^oC for ferric- and ferro- ILs, respectively. For both $Fe(CN)_6]^{3-/4-}$ samples, a second decomposition process was observed at 458 ^oC which, being absent for $[P_{14,6,6,6}][Cl]$, can be unambiguously attributed to the $Fe(CN)_6$ moiety. Sun et al. [31] reported similar behaviour in the TGA traces for phosphonium ILs based on organophosphate and organophosphinate anions.

4. Conclusions

The simple examples of functional electro-materials, based on redox active ionic liquids, shown here, demonstrate the possibility of creating new potentially useful materials with unique properties from easily available starting materials. These examples of building electrochemical functionality into ionic liquid structure are relatively straightforward from a synthetic perspective, but the likelihood of success (obtaining a RTIL) depends entirely on the nature of the anion and cation, therefore restricting synthesis to commercially available ions will inevitably severely limit the functional materials obtained. Notwithstanding, concerning the materials demonstrated here, the simple reversible electrochemistry, and their stability, bodes

well for their potential future application is energy storage devices (e.g. batteries and hybrid capacitors), sensors, redox catalysis and bio-electrochemistry.

5. Acknowledgments

L. G. would like to thank the Department of Education and Learning in Northern Ireland for a PhD Studentship. APD and GGW thank The Royal Society of London for an International Collaboration Grant. And all the Authors thank Dr Paula Douglas at the Polymer Processing Research Centre within QUB for performing the thermal analysis.

6. References

1. J. S., Wilkes, M. J. Zaworotko, Chem. Commun. 13 (1992) 965 - 967.

2. F. H. Hurley, T. P. Wier, Jr., US Patent 2,446,349 (1948).

3. H. L.Chum, V. R. Koch, L. L. Miller, R. A. Osteryoung, J. Am. Chem. Soc. 91 (1975) 3264 - 3265.

4. T. Welton, Chem. Rev. 99 (1999) 2071 - 2083.

5. J. Holbrey, K. R. Seddon, Clean Products and Processes 1 (1999) 223-236.

6. P. Wasserscheid, T.Welton; Ionic Liquids in Synthesis; Wiley, VCH: Weinheim, 2002.

7. M. J. Earle, S. P. Katdare, K. R. Seddon, Org. Lett., 6 (2004 707-710

8. J. H. Davis, Chem Lett. 33 (2004) 1072 -1077.

9. E. D. Bates, R. D. Mayton, I. Ntai, J. H. Davis, J. Am. Chem. Soc. 124 (2002) 926-927.

10. M. E. Williams, R.W. Murray, J. Phys Chem. B. 103 (1999) 10221-10227.

11. H, Masui, R. W. Murray, Inorg. Chem. 36 (1997) 5118 - 5126.

12. P. K. Bhowmik, H, Haesook, J. J. Cebe, R. A. Burchett, Liquid Crystals, 30 (2003) 1433 - 1440.

13. Y. Gao, B. Twamley, J. M. Shreeve, Inorg. Chem. 43 (2004) 3406 - 3412.

14. M. G. Kang, K. S. Ryu, S. H. Chanh, N. G. Park, ETRI 26 (2004) 26 647- 652.

15. X. E. Wu, L. Ma, M.X. Ding, L.X. Gao, Synlett 4 (2005) 607-610.

16, V. Strehmel, H. Rexhausen, P. Strauch, Tet. Lett. 49 (2008) 7143-7145.

17. P. Bonhote, A. P.Dias, N. Papageorgiou, K. Kalyanasundaram, M. Gratzel, Inorg. Chem. 35 (1996) 1168–1178.

18. R. E. D. Sesto, C. Corley, A. Robertson, J. S. Wilkes, J. Organomet. Chem. 690 (2005), 2536-2542.

19 K. R. Seddon, A., Stark, M. J.Torres Pure Appl. Chem. 72 (2000) 2275-2287.

20 K. Paduszyński, U. Domańska, J. Chem. Inf. Model 54 (2014) 1311-1324

21. K. J. Fraser, D. R. MacFarlane, Aust. J. Chem., 62 (2009) 309–321.

22. H. Vogel *Phys. Z.*, 22 (1921) 22, 645

23. G. Tamman, G. Hesse, Z. Anorg. Allg. Chem. 156 (1926) 245.

24. L. Wang J. Phys. Condens. Matter, 24 (2012) 155103.

25. C. L. Lagrost, D. Carrié, M. Vaultier, P. Hapiot, J. Phys. Chem. A, 107 (2003) 745 – 752.

26. V. Gutmann, G. Gritzner, K .Danksagmüller, Inorg. Chim. Acta. 17 (1976), 81- 86.

27. G. Gritzner, K. Danksagmüller, V.Gutmann; J. Electroanal. Chem. 72 (1976) 177-185.

28. G.Gritzner, D K.anksagmüller, V.Gutmann, J. Electroanal. Chem. 90 (1978) 203- 210.

29. D. Pletcher, R. E.Noftle, J. Electroanal. Chem. 293 (1990) 273-277.

30. F. Lucarelli, F Ricci , F, Caprio, F. Valgimigli, C. Scuffi, D. Moscone, G. Palleschi, J. Diabetes Sci. Technol. 6 (2012) 1172-81.

31. J. Sun, P. C. Howlett, D. R. MacFarlane, J. Lin, M. Forsyth, Electrochim. Acta, 54 (2008) 254-260.

Table / Figures Legends

Table 1 Glass transition and thermal degradation temperatures of the IL samples as recorded by DSC and TGA, respectively.

Figure 1 Structures of first stable room temperature ionic liquids [1].

Figure 2 Structure of $[P_{14,6,6,6}]_3[Fe(CN)_6]^{3/4-}$.

Figure 3 Collation of Arrhenius plots for $[P_{14,6,6,6}]_3[Fe(CN)_6]^{3-}$ and $[P_{6,6,6,14}]_4[Fe(CN)_6]^{4-}$ samples.

Figure 4 A cyclic voltammogram, recorded at a potential sweep rate of 100 mV/s, of 1.0 x 10^{-2} mol/L $[P_{14,6,6,6}]_3[Fe(CN)_6]^{3-}$ and ferrocene in acetonitrile containing 0.1 mol/L TBATFB.

Figure 5 Cyclic voltammograms, recorded at the potential sweep rates indicated, of 1.0 x 10^{-2} mol/L $[P_{14,6,6,6}]_3[Fe(CN)_6]^{3-}$ in acetonitrile containing 0.1 mol/L TBATFB.

Figure 6 Cyclic voltammograms, recorded at the potential sweep rates indicated, of 1.0 x 10^{-2} mol/L $[P_{14,6,6,6}]_4[Fe(CN)_6]^{4-}$ in acetonitrile containing 0.1 mol/L TBATFB.

Figure 7 Randles-Sevcik plots for the reduction and re-oxidation of 1.0 x 10^{-2} mol/L $[P_{14,6,6,6}]_3$ $[Fe(CN)_6]^{3-}$ in acetonitrile containing 0.1 mol/L TBATFB.

Figure 8 Cyclic voltammograms, recorded at the potential sweep rates indicated, of 1.0 x 10^{-2} mol/L $[P_{14,6,6,6}]_3[Fe(CN)_6]^{3-}$in $[P_{6,6,6,14}][NTf_2]$.

Figure 9 Cyclic voltammograms, recorded at the potential sweep rates indicated, of 1.0 x 10^{-2} mol/L $[P_{14,6,6,6}]_4[Fe(CN)_6]^{4-}$in $[P_{6,6,6,14}][NTf_2]$.

Figure 10 Randles-Sevcik plots for the reduction and re-oxidation of $[P_{14,6,6,6}]_3$ $[Fe(CN)_6]^{3-}$ in $[P_{6,6,6,14}][NTf_2]$.

Figure 11 Randles-Sevcik plots for the reduction and re-oxidation of $[P_{14,6,6,6}]_4$ $[Fe(CN)_6]^{4-}$ in $[P_{6,6,6,14}][NTf_2]$.

Figure 12 A cyclic voltammogram of 4.6 x 10^{-3} mol/L $[P_{14,6,6,6}]_4$ $[Fe(CN)_6]^{4-}$ recorded at a potential sweep rate of 10 mV/s in 0.1 M KCl in 5 % (w/v) CTAB and 0.1 mol/L PBS.

Table 1

Sample	Synthesis	T_g (°C)	T_{onset} (°C)	T_{2nd}
$[P_{14,6,6,6}]_3[Fe(CN)_6]^{3-}$	ACN / water (1:1)	-51	413	458
$[P_{14,6,6,6}]_3[Fe(CN)_6]^{3-}$	ACN / water (1:2)	-54	-	-
$[P_{14,6,6,6}]_3[Fe(CN)_6]^{3-}$	DMF / water (1:1)	-53	-	-
$[P_{14,6,6,6}]_3[Fe(CN)_6]^{3-}$	Acetone / water (1:1)	-54	-	-
$[P_{14,6,6,6}]_4[Fe(CN)_6]$	ACN / water (1+1)	-56 -70*	431	458
$[P_{14,6,6,6}][NTf_2]$	DCM/ water	-	425	-
$[P_{14,6,6,6}][Cl]$	-	-56*		

* [18]

Figure 1

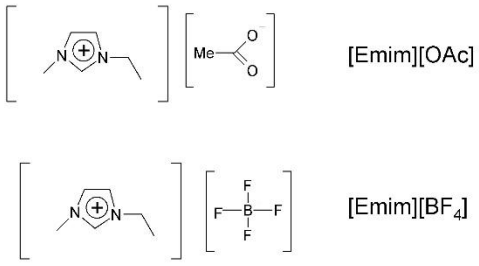

Figure 2

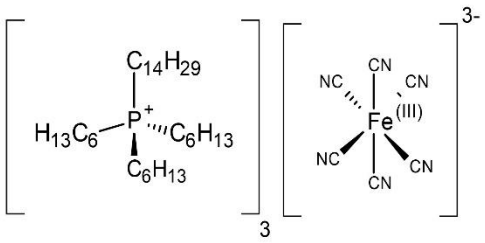

Figure 3

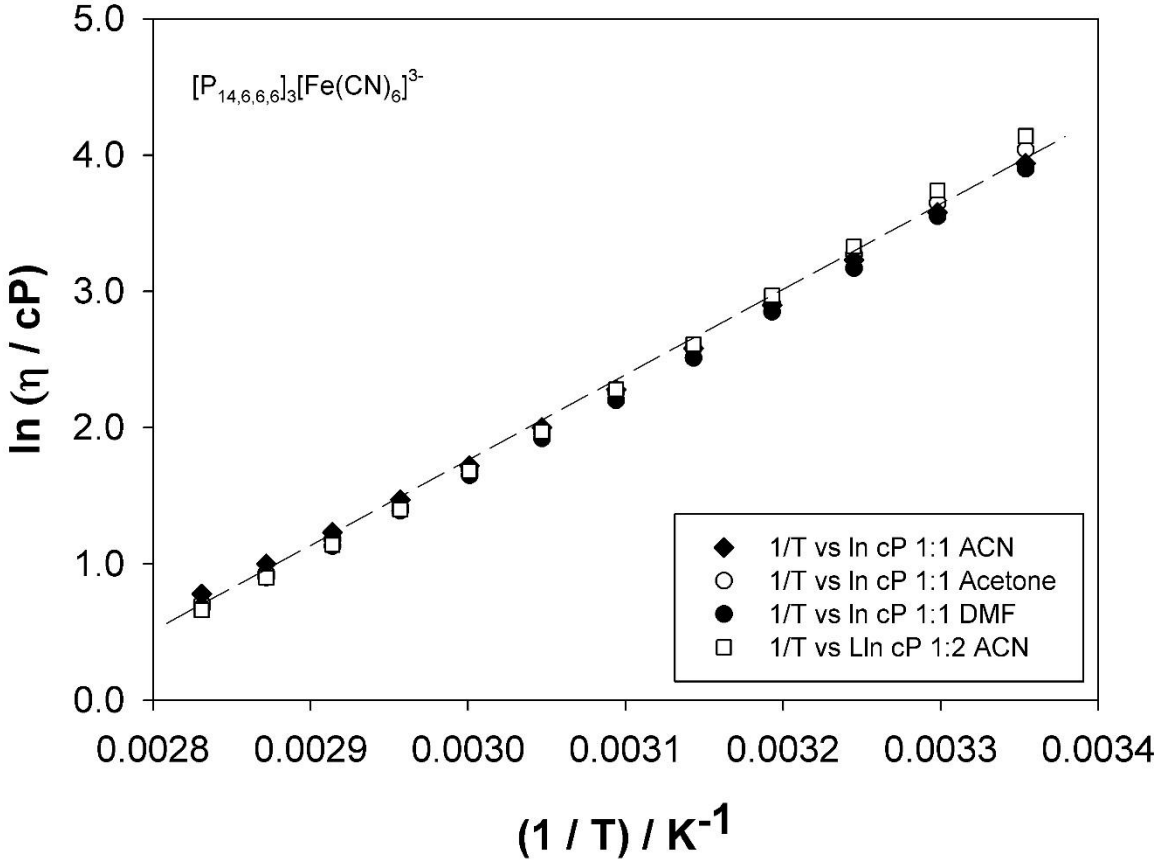
[P14,6,6,6]3[Fe(CN)6]3-
ln (η / cP)
(1 / T) / K-1
5.0
4.0
3.0
2.0
1.0
0.0
0.0028
0.0029
0.0030
0.0031
0.0032
0.0033
0.0034
1/T vs ln cP 1:1 ACN
1/T vs ln cP 1:1 Acetone
1/T vs ln cP 1:1 DMF
1/T vs LIn cP 1:2 ACN

Figure 4

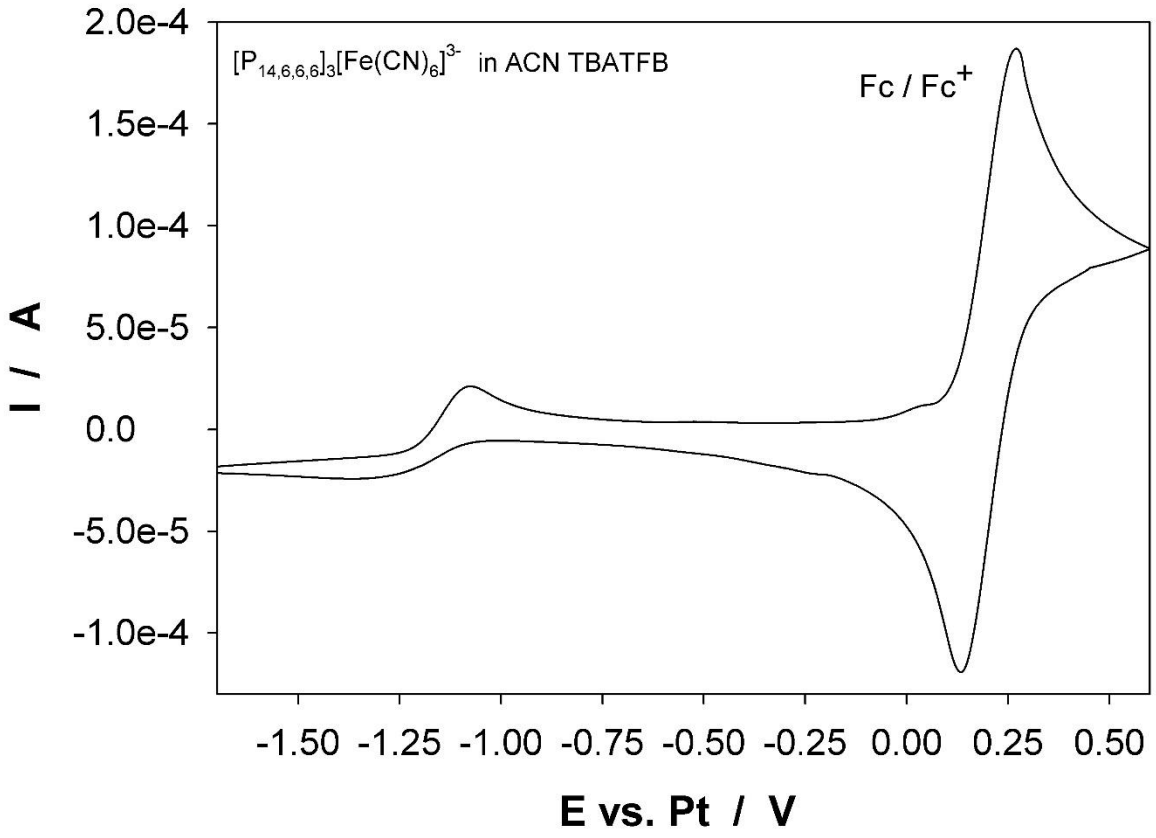
2.0e-4
1.5e-4
1.0e-4
5.0e-5
0.0
-5.0e-5
-1.0e-4
I / A
[P14,6,6,6]3[Fe(CN)6]3- in ACN TBATFB
Fc / Fc+
-1.50 -1.25 -1.00 -0.75 -0.50 -0.25 0.00 0.25 0.50
E vs. Pt / V

Figure 5

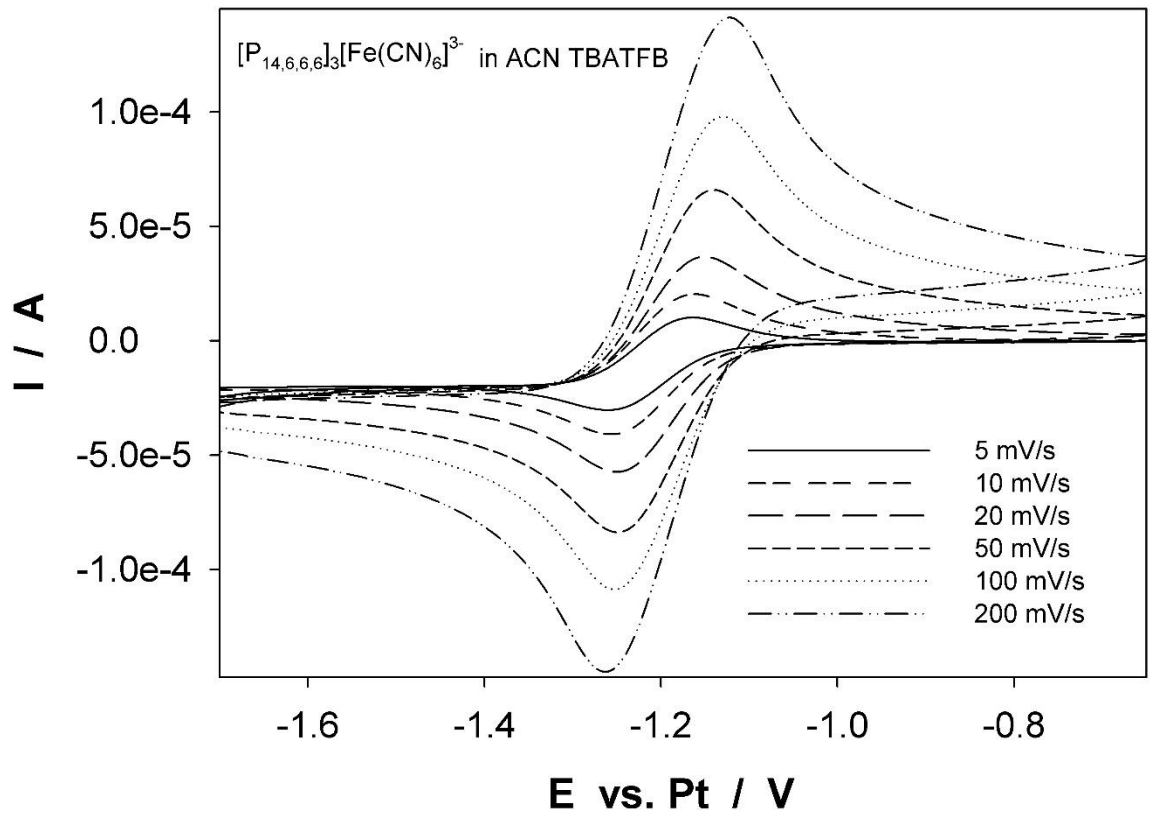
[P14,6,6,6]3[Fe(CN)6]3- in ACN TBATFB
1.0e-4
5.0e-5
0.0
-5.0e-5
-1.0e-4
I / A
-1.6
-1.4
-1.2
-1.0
-0.8
E vs. Pt / V
5 mV/s
10 mV/s
20 mV/s
50 mV/s
100 mV/s
200 mV/s

Figure 6

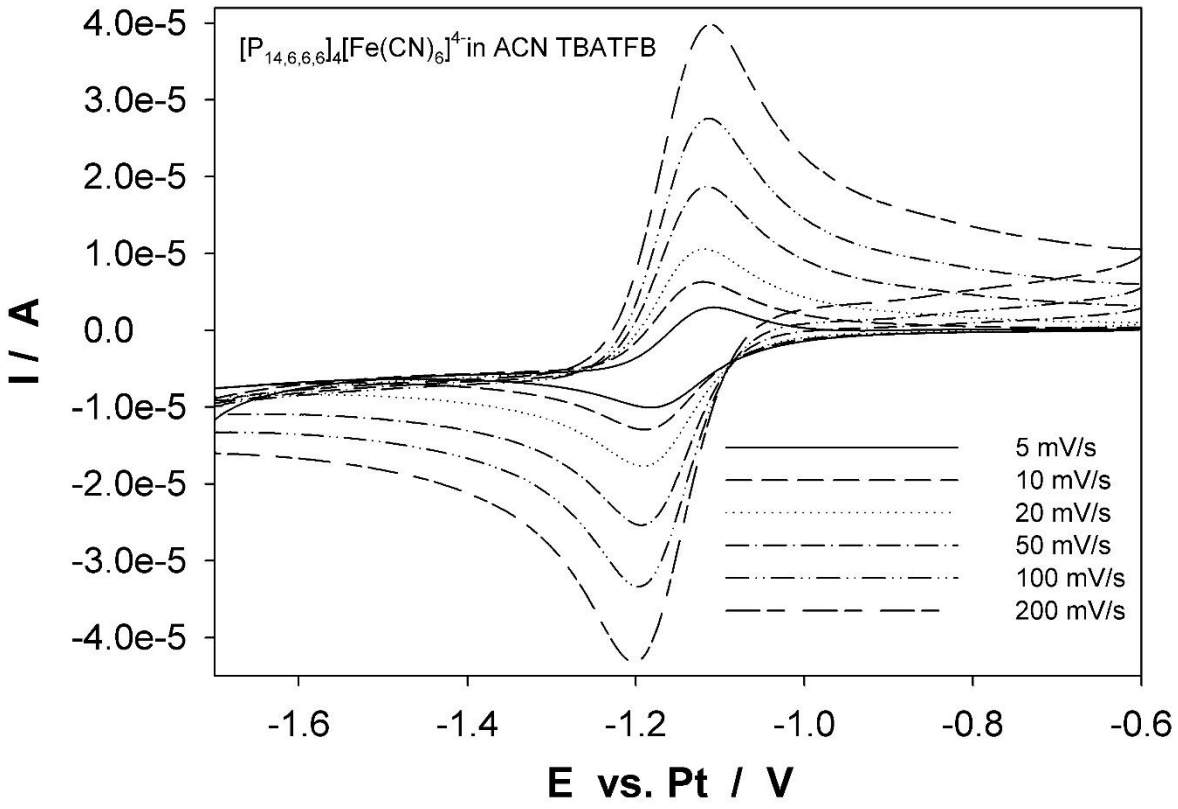
[P14,6,6,6]4[Fe(CN)6]4- in ACN TBATFB
4.0e-5
3.0e-5
2.0e-5
1.0e-5
0.0
-1.0e-5
-2.0e-5
-3.0e-5
-4.0e-5
I / A
-1.6
-1.4
-1.2
-1.0
-0.8
-0.6
E vs. Pt / V
5 mV/s
10 mV/s
20 mV/s
50 mV/s
100 mV/s
200 mV/s

Figure 7

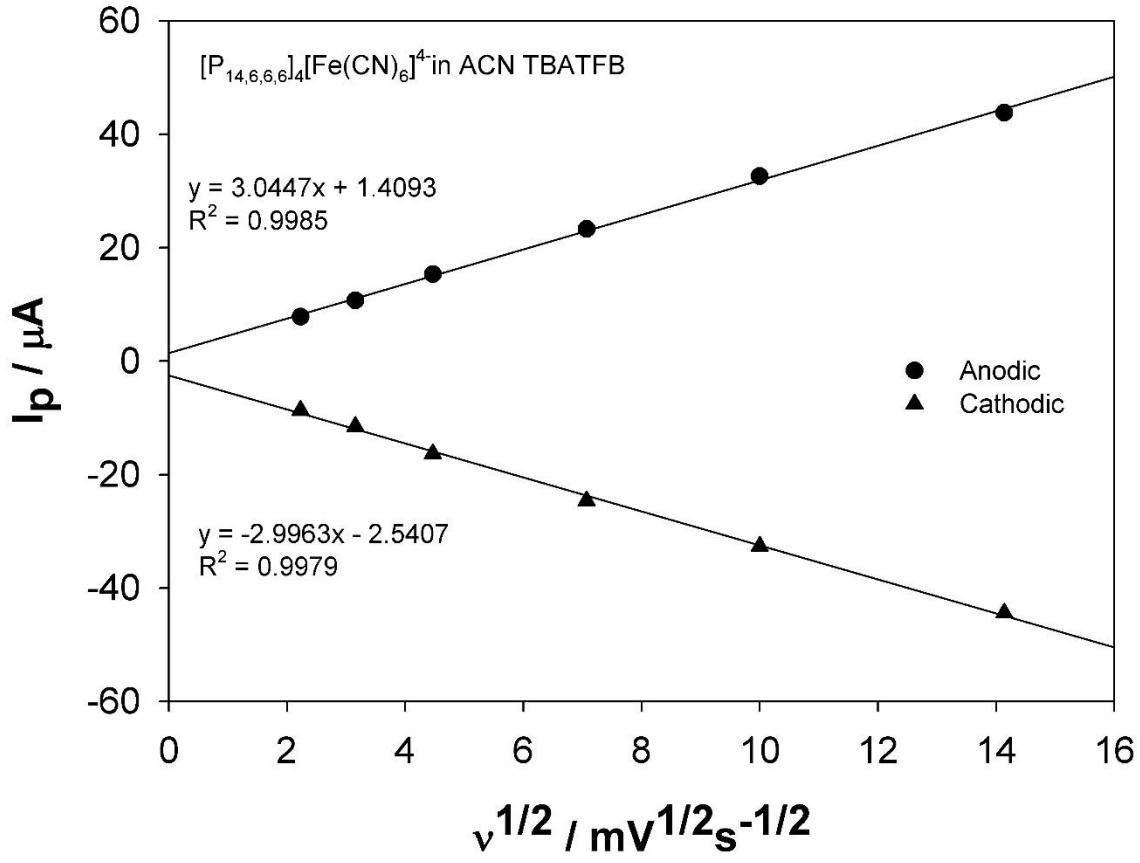
[P14,6,6,6]4[Fe(CN)6]4- in ACN TBATFB
y = 3.0447x + 1.4093
R2 = 0.9985
y = -2.9963x - 2.5407
R2 = 0.9979
Anodic
Cathodic
Ip / µA
ν1/2 / mV1/2s-1/2
60
40
20
0
-20
-40
-60
0
2
4
6
8
10
12
14
16

Figure 8

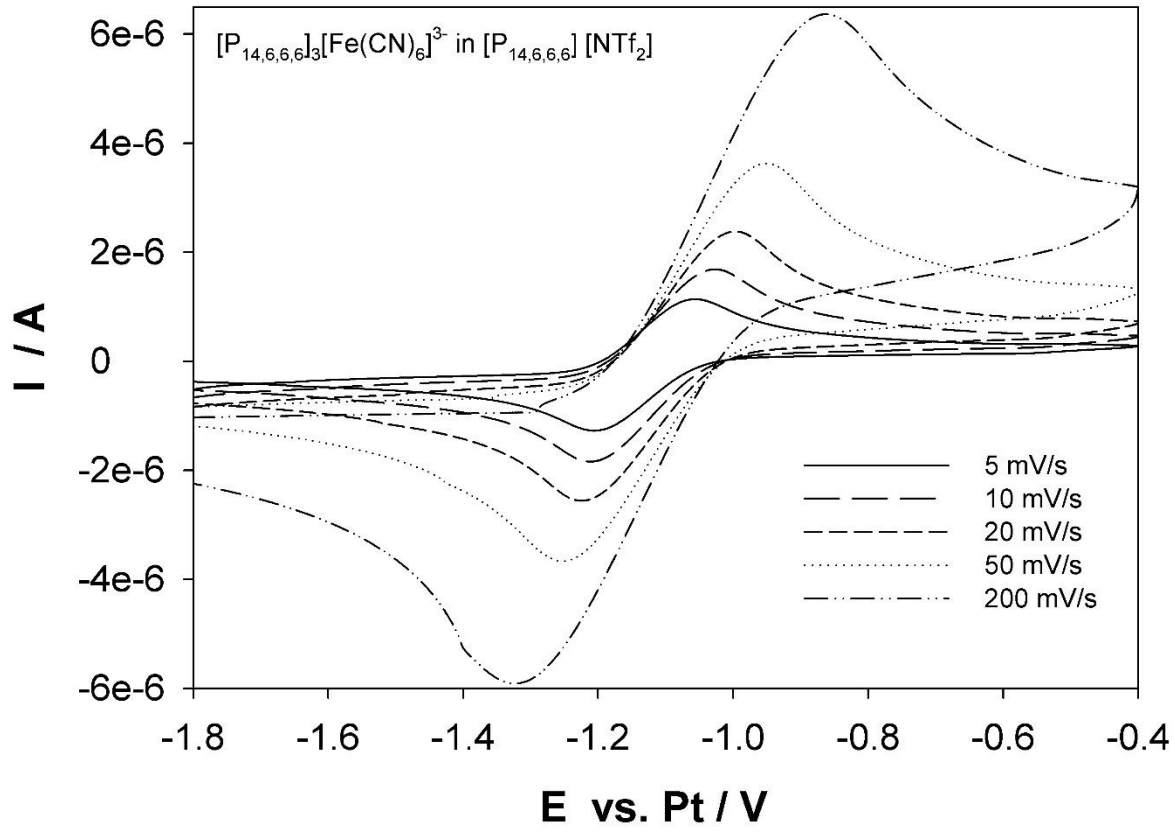
[P14,6,6,6]3[Fe(CN)6]3- in [P14,6,6,6] [NTf2]
6e-6
4e-6
2e-6
0
-2e-6
-4e-6
-6e-6
I / A
-1.8
-1.6
-1.4
-1.2
-1.0
-0.8
-0.6
-0.4
E vs. Pt / V
5 mV/s
10 mV/s
20 mV/s
50 mV/s
200 mV/s

Figure 9

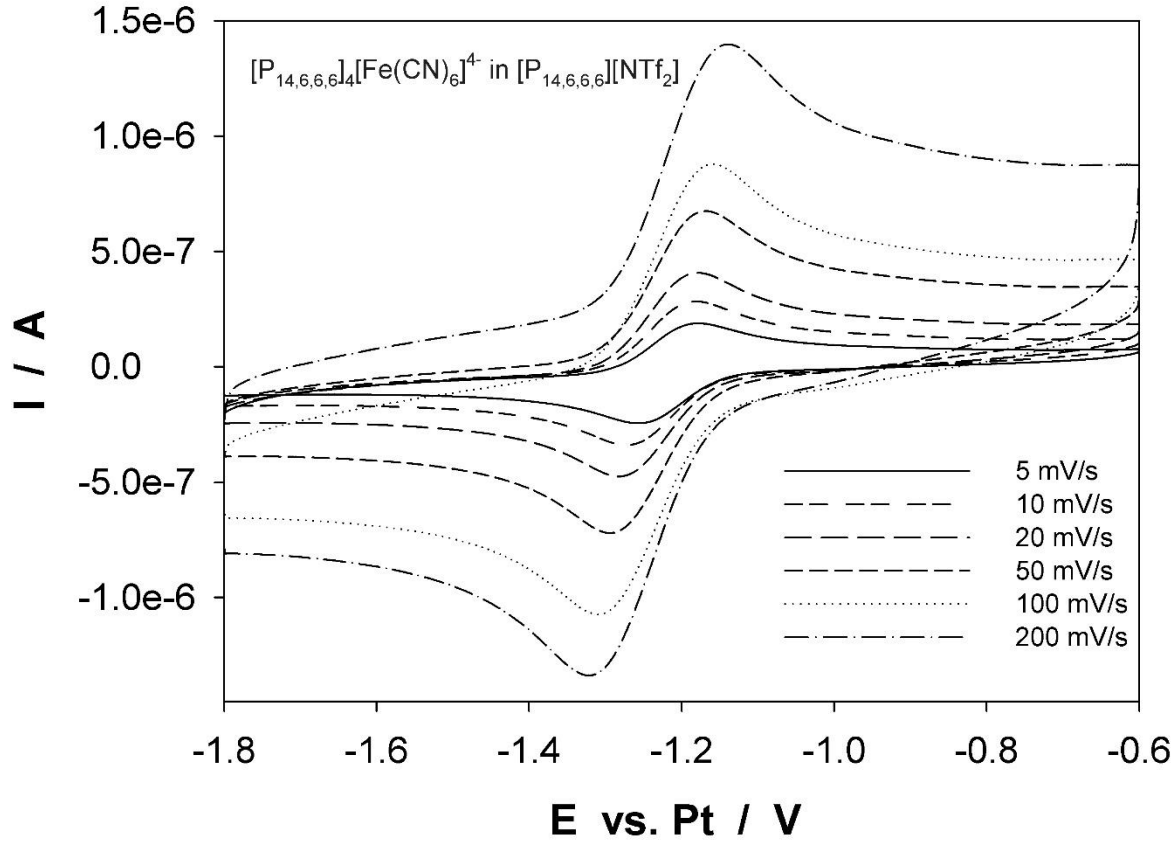
[P14,6,6,6]4[Fe(CN)6]4- in [P14,6,6,6][NTf2]
1.5e-6
1.0e-6
5.0e-7
0.0
-5.0e-7
-1.0e-6
I / A
-1.8
-1.6
-1.4
-1.2
-1.0
-0.8
-0.6
E vs. Pt / V
5 mV/s
10 mV/s
20 mV/s
50 mV/s
100 mV/s
200 mV/s

Figure 10

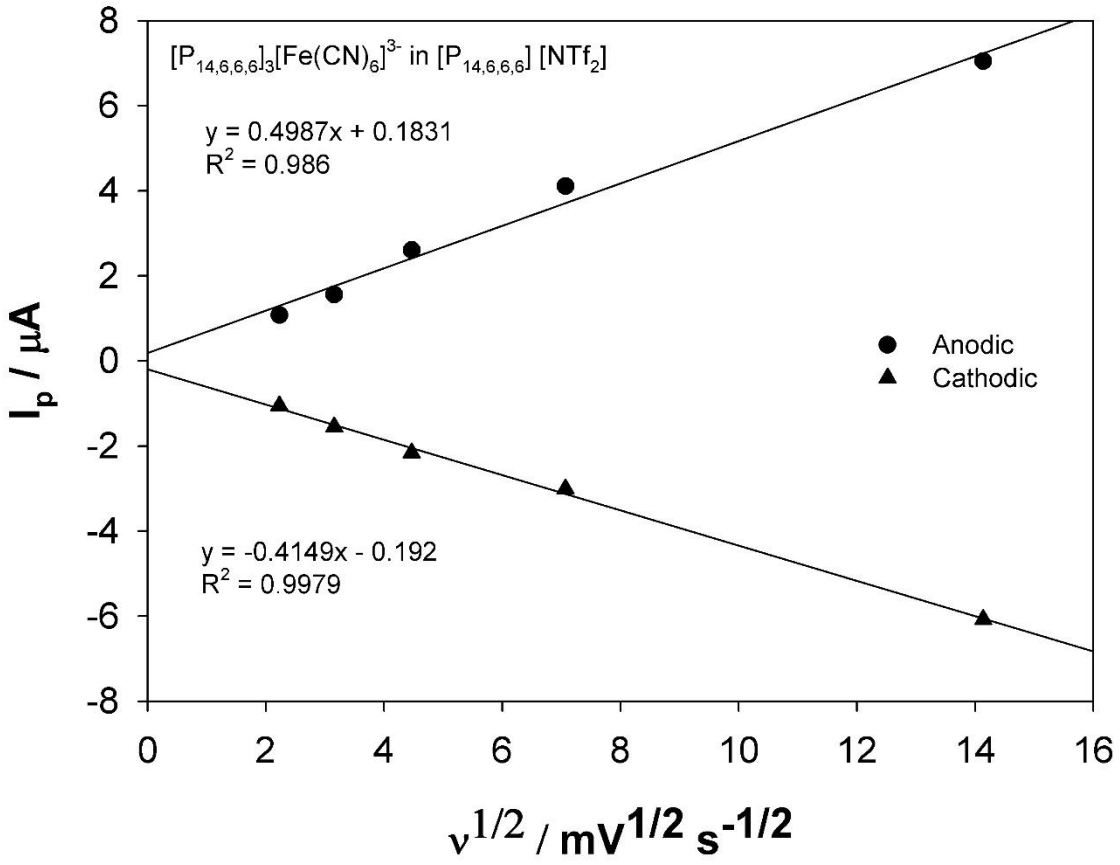
[P14,6,6,6]3[Fe(CN)6]3- in [P14,6,6,6] [NTf2]
y = 0.4987x + 0.1831
R2 = 0.986
y = -0.4149x - 0.192
R2 = 0.9979
Anodic
Cathodic
Ip / µA
ν1/2 / mV1/2 s-1/2
8
6
4
2
0
-2
-4
-6
-8
0
2
4
6
8
10
12
14
16

Figure 11

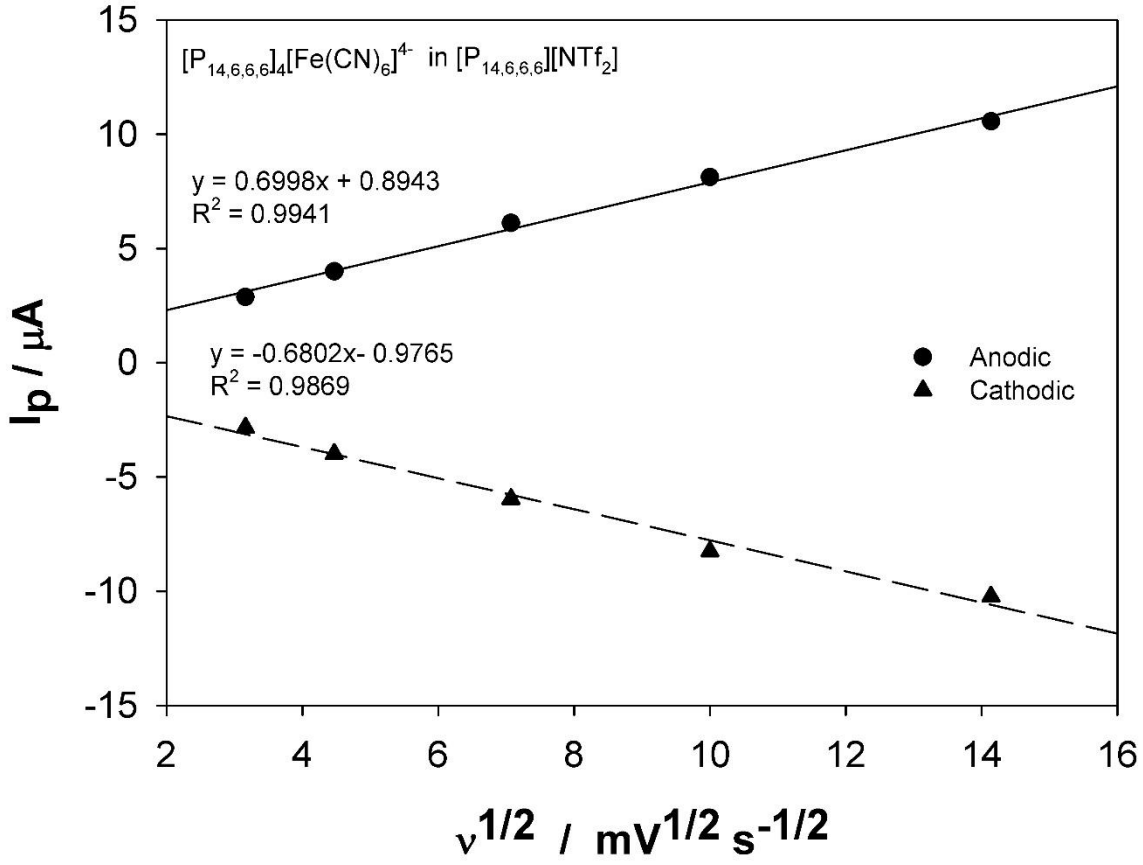
[P14,6,6,6]4[Fe(CN)6]4- in [P14,6,6,6][NTf2]
y = 0.6998x + 0.8943
R2 = 0.9941
y = -0.6802x- 0.9765
R2 = 0.9869
Anodic
Cathodic
Ip / µA
ν1/2 / mV1/2 s-1/2
15
10
5
0
-5
-10
-15
2
4
6
8
10
12
14
16

Figure 12

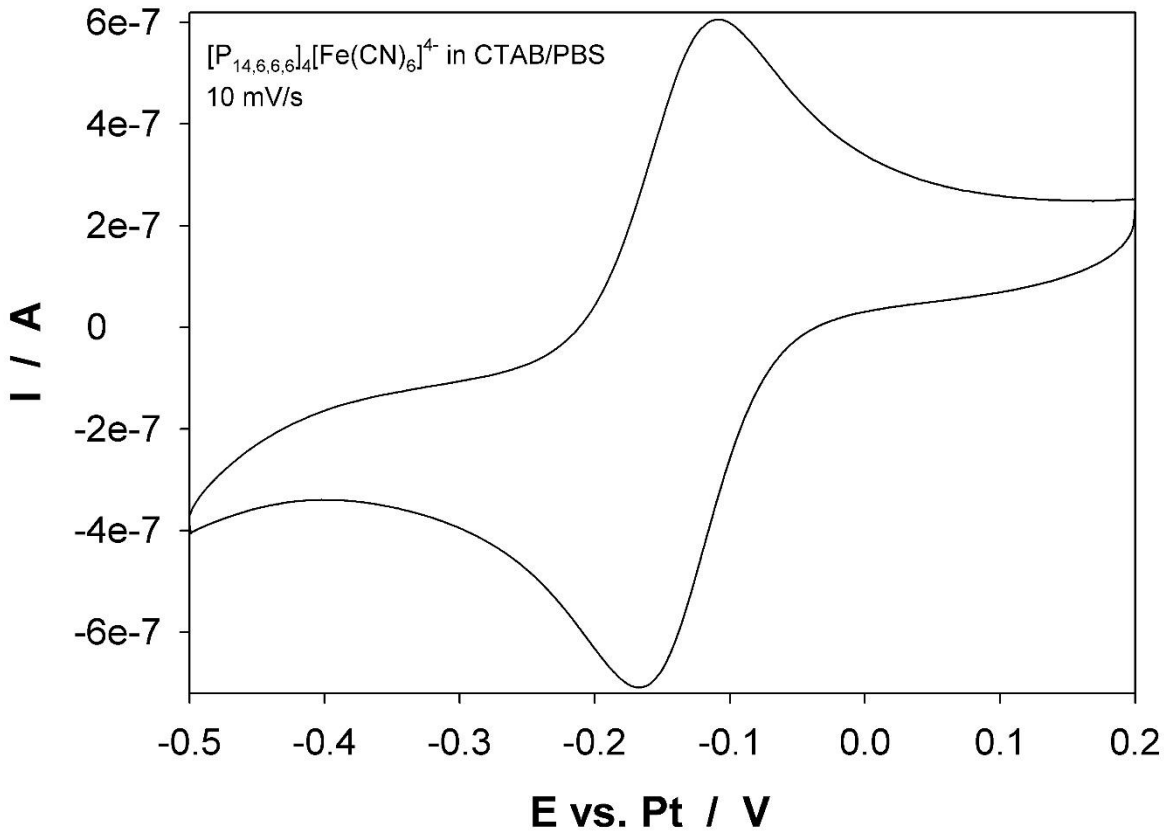
[P14,6,6,6]4[Fe(CN)6]4- in CTAB/PBS
10 mV/s
6e-7
4e-7
2e-7
0
-2e-7
-4e-7
-6e-7
I / A
-0.5
-0.4
-0.3
-0.2
-0.1
0.0
0.1
0.2
E vs. Pt / V